Development and Validation of a Self-Aligning Knee Exoskeleton With Hip Rotation Capability

Guotao Li, *Member, IEEE*, Xu Liang, Huijuan Lu, Tingting Su, and Zeng-Guang Hou, *Fellow, IEEE*

Abstract— **The self-aligning capability of an exoskeleton is important to ensure wearing comfort, and the delicate motion ability of the exoskeleton is essential for motion assistance. Designing a self-aligning exoskeleton that offers improved wearing comfort and enhanced motion-assistance functions remains a challenge. This paper proposes a novel spatial self-aligning mechanism for a knee exoskeleton to enable simultaneous assistance in the flexion and extension (FE) of the knee joint and the internal and external rotation (IER) of the hip joint. Additionally, considering the misalignment of the human-robot joint axes, a kinematic model of the knee exoskeleton is established and analyzed to demonstrate the kinematic compatibility of the exoskeleton. Furthermore, a global torque manipulability (GTM) index is proposed to evaluate the effects of dimensional parameters on the exoskeleton's performance, and then the knee exoskeleton is optimized according to the GTM index. Finally, experiments are conducted to validate the performance of the proposed exoskeleton. The experimental results show that during knee FE and hip IER, the proposed exoskeleton exhibits lower interaction forces and torques than existing exoskeletons.**

Index Terms— **Knee exoskeleton, self-aligning mechanism, kinematic compatibility, optimization.**

I. INTRODUCTION

THE human knee is the largest joint in the human body. It is important for almost any exercise, including, walk-ing, running, cycling, and swimming [1], [2]. However, the knee is highly vulnerable to sports trauma, stroke, and other diseases [3]. Therefore, numerous researchers have investigated the development of knee exoskeletons [4].

Traditionally, the knee joint is simplified as a simple rotary joint in exoskeleton designs, and numerous knee exoskeletons have been developed according to this simplification [5], [6], [7], [8], [9], [11], [12]. However, the earlier exoskeleton designs [5], [6], [7], [8], [9], [11], [12] did not consider the misalignment of the human-robot joint axes. Owing to the anatomical structure and soft tissue deformation of the knee joint, human-robot joint axis misalignment produces undesirable interaction forces between the exoskeleton and the human joint, which may exert pressure on the user's skin and reduce comfort [13].

Numerous design strategies have been proposed to address the misalignment of the human-robot joint axes. The performance of these methods depends on whether the exoskeleton is soft [14], rigid-soft [15] or rigid [16]. Soft exoskeletons and rigid-soft hybrid exoskeletons usually sacrifice loading capabilities to improve wearing comfort. Therefore, this paper focuses on rigid self-aligning exoskeletons to ensure both loading capability and wearing performance.

Different self-aligning mechanisms of rigid knee exoskeletons have been proposed and developed to solve the problem of human-robot joint axis misalignment. For example, considering the knee rolling/sliding displacement, Wang et al. designed an adaptive knee exoskeleton based on the cam mechanism [17]. Ergin and Patoglu proposed a self-adjusting joint based on the 3-RRP (3-Revolute-Revolute-Prismatic) mechanism for knee exoskeletons [18]. Saccares et al. proposed a modular knee exoskeleton based on two parallelogram mechanisms to adapt to the knee's instantaneous center of rotation, but the authors did not prove its kinematic compatibility of the exoskeleton [19]. Scholars have developed different comfort-centred knee exoskeletons based on a rolling-joint-based mechanism for walking assistance [20], [21]. By adding passive degrees of freedom to human-robot closed-loop kinematic chains, Sarkisian et al. proposed a novel self-aligning knee exoskeleton [22]. Later, Sarkisian et al. demonstrated the effectiveness of the self-aligning knee exoskeleton by evaluating the performance and comfort through experimentation [23]. However, all of the above designs are based on planar self-aligning mechanisms, which cannot adapt to the instantaneous rotation center of the knee joint in a three-dimensional space.

Addressing human-robot misalignment via spatial self-aligning mechanisms has been an active research area. For

example, Cempini et al. proposed a method for analyzing the self-aligning mechanism of rigid exoskeletons and provided some design examples. However, the authors did not provide a general method for implementing such mechanisms [24]. Agarwal et al. developed a spatial self-aligning mechanism configuration for a thumb exoskeleton, but they did not verify the kinematic compatibility of the exoskeleton in different directions [25]. Recently, our team proposed an adaptive index exoskeleton and an adaptive thumb exoskeleton based on spatial self-aligning mechanisms and performed theoretical and experimental validation [26], [27]. However, the configurations of these spatial self-aligning mechanisms cannot be directly applied to knee exoskeletons, because the strap attachments and fixation devices of knee exoskeletons differ from hand exoskeletons. The process of designing spatial self-aligning mechanisms for knee joint exoskeletons remains unclear.

This paper proposes a spatial self-aligning mechanism for a knee exoskeleton. The mechanism can simultaneously provide the flexion and extension (FE) of the knee joint and the internal and external rotation (IER) of the hip joint. To the best of the authors' knowledge, this is the first study to propose a knee exoskeleton that can simultaneously assist in the knee FE and the hip IER. Stroke rehabilitation needs passive and active assistance. Stroke patients in the soft paralysis stage have muscle weakness and need passive rehabilitation training [28]. To solve the passive rehabilitation problem, this paper focuses on the mechanism design of the exoskeleton and its passive assistance function. The contributions of this paper are summarized below.

- A spatial self-aligning exoskeleton that can simultaneously assist in the FE of the knee joint and the IER of the hip joint is proposed to improve wearing comfort.
- Considering the misalignment of the human-robot joint axes, a kinematic model of the knee exoskeleton is established and analyzed to show the kinematic compatibility of the knee exoskeleton.
- An optimization method of the knee exoskeleton is proposed based on a global torque manipulability index to improve the torque transmission ability.

The remainder of this paper is organized as follows. Section II presents a knee exoskeleton. Section III analyzes the kinematic compatibility. Section IV optimizes the knee exoskeleton. Section V presents the experiments. Sections VI and VII discuss and conclude the paper.

II. KNEE EXOSKELETON DESIGN

A. Design Motivation

The human knee joint has three movements: knee FE movement, knee varus/valgus, and knee IER [1], [2]. Among these, knee FE movement is the primary motion, and it includes a wide range of motions. The knee varus/valgus angle is fixed for each user and only has a small variation range of approximately 5°-10°. The knee varus/valgus may affect the hip IER movement. However, when the knee is flexed, the knee varus/valgus and the hip IER movement jointly generate a motion of the shank. Assuming that the user's knee
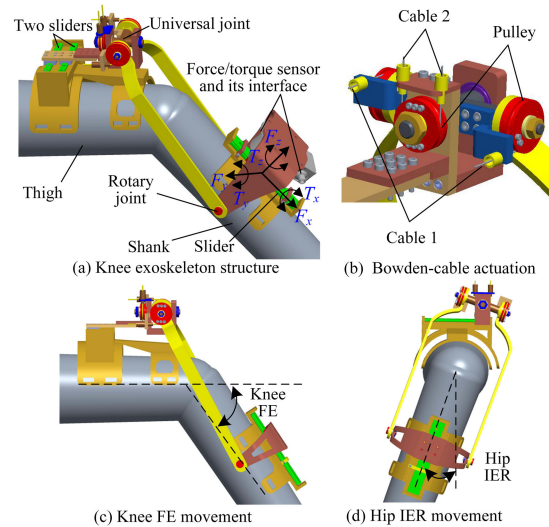

Fig. 1. Design of a knee exoskeleton. (a) and (b) Overall structure and actuation unit. (c) and (d) Knee FE movement and hip IER movement.

varus/valgus is normal, we can neglect the knee varus/valgus and only consider the hip IER movement when designing the exoskeleton. Knee IER typically occurs when the knee is flexed, and the assistance for knee IER is typically achieved through an ankle exoskeleton, rather than a knee exoskeleton. In contrast, hip IER can be assisted by a knee exoskeleton rather than a hip exoskeleton. Thus, both knee FE and hip IER can be assisted by a knee exoskeleton, and their simultaneous movement may also be assisted by a knee exoskeleton.

Moreover, a knee exoskeleton that can simultaneously assist knee FE and hip IER movements could broaden its application scope. First, it is best for the rehabilitation robot to be able to independently assist each joint of the patient to perform different rehabilitation training [28], [29]. The proposed knee exoskeleton can increase the function of hip IER assistance and thus improve the rehabilitation effects of the exoskeleton. Second, incorporating hip IER movement can enhance walking agility during walking assistance [30]. Thus, the proposed knee exoskeleton also has the potential to enhance walking assistance performance.

The anatomical structure of the knee joint determines that its instantaneous center of rotation may have three translations across its three anatomical planes. Thus, the proposed exoskeleton should be able to adapt to the instantaneous rotation center of the knee joint. In addition, a compact and lightweight structure is also important for the portability and usability of knee exoskeletons. Therefore, this paper proposes a portable, comfort-centric knee exoskeleton with hip IER capability.

B. Design of a Self-Aligning Knee Exoskeleton

The overall structure of the knee exoskeleton with a force/torque sensor is shown in Fig. 1(a). The knee exoskeleton is composed of a universal joint, a rotary joint, two sliding joints, and a force/torque sensor. Among these components, the rotary joint and two sliding joints of the knee exoskeleton are passive, and the universal joint is an active joint actuated by a Bowden-cable transmission system. As shown in Fig. 1(b),
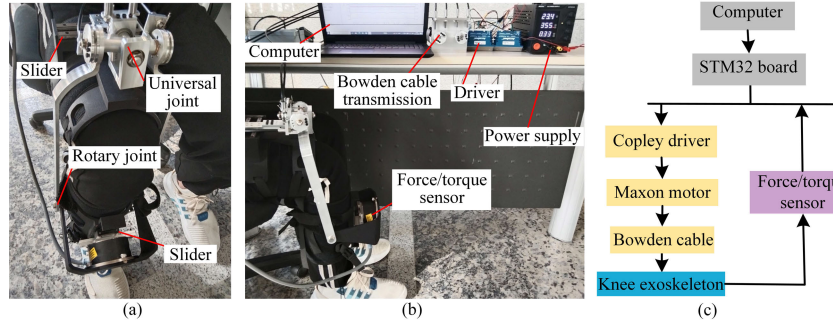
Fig. 2. Knee exoskeleton system. (a) Knee exoskeleton prototype. (b) Actuation and control system. (c) Hardware system configuration.

cable 1 and the corresponding two pulleys are used to actuate a rotary joint of the universal joint corresponding to the knee FE, and cable 2 and the corresponding pulley are used to actuate the other rotary joint corresponding to the hip IER. To enhance structural strength, two sliders form the sliding joint on the thigh, while a larger slider constitutes the sliding joint on the shank. The directions of the six forces and torques of the force/torque sensor are depicted in Fig. 1(a), where the axes of force F_z and torque T_z align with the axis of the force/torque sensor, and the axes of force F_x and torque T_x are parallel to the slider on the shank.

Figures 1(c) and 1(d) show a knee exoskeleton without a force/torque sensor. The knee exoskeleton can actuate the knee FE movement and the hip IER movement. The knee varus/valgus angle is fixed for each user. In this paper, the knee varus/valgus angle of the user is assumed to be normal, specifically 0°. Thus, the movement of the shank around the femoral axis of the thigh in Fig. 1(d) can be used to represent the hip IER movement.

C. Hardware System of the Knee Exoskeleton

Figure 2(a) displays the fabricated knee exoskeleton, in which the two rotary joints in the universal joint are driven by two Maxon motors through the Bowden cable transmission. The other rotary joint and sliders are passive joints. Fig. 2(b) shows the entire exoskeleton system, composed of a knee exoskeleton, a computer, an STM32 development board, two Copley drivers, two Maxon motors, and a power supply. The entire exoskeleton system weighs ~2.15 kg. The STM32 development board and the two Copley drivers are used to drive the two Maxon motors. In addition, a six-axis force and torque sensor (ATI-Gamma, USA) is installed at the shank to measure the interaction forces between the user and the exoskeleton. To clearly illustrate the system, Fig. 2(c) shows the whole hardware system configuration of the knee exoskeleton.

III. KINEMATIC COMPATIBILITY ANALYSIS

A. Kinematics of Knee Exoskeleton

1) Forward Kinematics of Knee Exoskeleton: To establish the kinematic model of the exoskeleton, the definitions are given as follows. $q_i (i = 1, \ldots, 5)$ denotes the exoskeleton joint variables, where $q_i (i = 1, 5)$ are the displacement variables of the prismatic joints and $q_i (i = 2, 3, 4)$ are the angle variables of the rotary joint. $\tilde{q}_1$ denotes the hip IER joint angle and
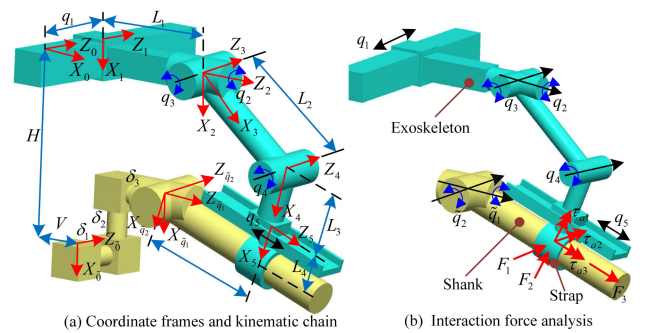

Fig. 3. Coordinate frames of the closed-loop system and the interaction force analysis between the exoskeleton and human limb.

$\tilde{q}_2$ as the knee FE joint angle. $L_i (i = 1, \ldots, 4)$ denotes the lengths of the knee exoskeleton link i, where L_4 is the distance between the axis of sliding joint q_5 and the center axis of the human knee joint. L_5 denotes the corresponding length along the shank between the human knee center and the Velcro strap.

Figure 3(a) shows that the knee exoskeleton is connected with the human hip and knee joints through a Velcro strap to form a closed-loop system. The knee exoskeleton is modeled as a prismatic-universal-rotational-prismatic mechanism. The human hip IER joint $\tilde{q}_1$ and knee FE joint $\tilde{q}_2$ are orthogonal to form a universal joint. Considering that the instantaneous center of rotation of the knee joint has three translations in its three anatomical planes, as shown in Fig. 3(a), the model considers the relative displacements $(\delta_1, \delta_2, \delta_3)$. Thus, knee FE and hip IER are modeled according to the functionalities of a universal joint with three relative displacements of the instantaneous center of rotation. As shown in Fig. 3(a), according to the modified Denavit-Hartenberg (D-H) method, the coordinate frames of the kinematic chain $(q_1 - q_2 - q_3 - q_4 - q_5)$ of the knee exoskeleton and the kinematic chain $(\tilde{q}_1 - \tilde{q}_2 - q_5)$ of the human knee can be established. $\{X_0, Y_0, Z_0\}$ is the reference coordinate frame of the whole human-robot system. The origins of coordinate frames $\{X_{\tilde{0}}, Y_{\tilde{0}}, Z_{\tilde{0}}\}$ and $\{X_{\tilde{q}_1}, Y_{\tilde{q}_1}, Z_{\tilde{q}_1}\}$ represent the human knee centers before and after position variations, respectively. The displacement vector between the origins of coordinate frame $\{X_0, Y_0, Z_0\}$ and coordinate frame $\{X_{\tilde{0}}, Y_{\tilde{0}}, Z_{\tilde{0}}\}$ is $[V, H, 0]^T$, where V and H are two distance parameters of the human-robot system. According to the modified D-H method, the D-H parameters of the human-robot system are listed in Tables I and II.

By defining $\mathbf{q} = [q_1, q_2, q_3, q_4, q_5]^T$, $\tilde{\mathbf{q}} = [\tilde{q}_1, \tilde{q}_2]^T$, and $\boldsymbol{\delta} = [\delta_1, \delta_2, \delta_3]^T$, the closed-loop kinematic equation of the

TABLE I
KNEE EXOSKELETON CHAIN'S D-H PARAMETERS

i	α_{i-1}	a_{i-1}	d_i	θ_i
1	0	0	q_1	90°
2	90°	0	L_1	q_2
3	−90°	0	0	q_3
4	0	L_2	0	q_4
5	90°	L_3	q_5	0

TABLE II
HUMAN KNEE CHAIN'S D-H PARAMETERS

i	α_{i-1}	a_{i-1}	d_i	θ_i
$\tilde{0}$	0	0	0	90°
$\tilde{1}$	90°	0	0	$\tilde{q}_1$
$\tilde{2}$	−90°	0	0	$\tilde{q}_2$
$\tilde{3}$	90°	$-L_4$	L_5	0

knee exoskeleton and human knee system can be expressed as

$$^0_5\mathbf{T}^E(\mathbf{q}) = {}^0_5\mathbf{T}^H(\tilde{\mathbf{q}}, \boldsymbol{\delta}) \tag{1}$$

where $^0_5\mathbf{T}^E(\mathbf{q})$ represents the kinematic equation of the knee exoskeleton, and $^0_5\mathbf{T}^H(\tilde{\mathbf{q}}, \boldsymbol{\delta})$ represents the kinematic equation of the human limb. {0} denotes coordinate frame $\{X_0, Y_0, Z_0\}$. {5} denotes coordinate frame $\{X_5, Y_5, Z_5\}$ of the knee exoskeleton, which is the same as the coordinate frame $\{\tilde{3}\}$ of the human knee joint. {E} and {H} denote the kinematic chains of the knee exoskeleton and the human limb, respectively.

Based on the modified D-H method [27] and D-H parameters listed in Table I, $^0_5\mathbf{T}^E(\mathbf{q})$ can be expressed as

$$^0_5\mathbf{T}^E(\mathbf{q}) = {}^0_1\mathbf{T}^1_2\mathbf{T}^2_3\mathbf{T}^3_4\mathbf{T}^4_5\mathbf{T} \tag{2}$$

where $^{i-1}_i\mathbf{T}$ is the homogeneous transformation matrix based on the parameters presented in Table I.

To establish the kinematic equation of the human knee joint, we first transform coordinate frame {0} to coordinate frame $\{\tilde{0}\}$. Then, based on the modified D-H method and D-H parameters listed in Table II, the kinematic equation $^0_5\mathbf{T}^H(\tilde{\mathbf{q}}, \boldsymbol{\delta})$ of the human knee kinematic chain can be expressed as

$$^0_5\mathbf{T}^H(\tilde{\mathbf{q}}) = {}^0_{\tilde{0}}\bar{\mathbf{T}}^{\tilde{0}}_{\tilde{1}}\mathbf{T}^{\tilde{1}}_{\tilde{2}}\mathbf{T}^{\tilde{2}}_{\tilde{3}(5)}\mathbf{T} \tag{3}$$

where $^0_{\tilde{0}}\bar{\mathbf{T}}$ can be obtained as $^0_{\tilde{0}}\bar{\mathbf{T}} = \mathbf{Trans}(V + \delta_3, H - \delta_2, \delta_1)^0_{\tilde{0}}\mathbf{T}$ based on the homogeneous transformation method, and $^{\tilde{i}-1}_{\tilde{i}}\mathbf{T}$ is the homogeneous transformation matrix based on the parameters in Table II.

Based on (1)-(3), the IER angle $\tilde{q}_1$ of the human hip joint and the FE angle $\tilde{q}_2$ of the knee joint can be calculated based on the exoskeleton joints q_i. The expression can be written as

$$\begin{pmatrix} \tilde{q}_1 \\ \tilde{q}_2 \\ \delta_1 \\ \delta_2 \\ \delta_3 \end{pmatrix}$$
$$= \begin{pmatrix} q_2 \\ q_3 + q_4 \\ q_1 - s_2((q_5 - L_5)s_{34} + (L_3 + L_4)c_{34} + L_2c_3) \\ H - c_2((q_5 - L_5)s_{34} + (L_3 + L_4)c_{34} + L_2c_3) \\ L_1 - V + (q_5 - L_5)c_{34} - (L_3 + L_4)s_{34} - L_2s_3 \end{pmatrix} \tag{4}$$

where $c_i = \cos q_i$, $s_i = \sin q_i$, $c_{ij} = \cos(q_i + q_j)$, and $s_{ij} = \sin(q_i + q_j)$.

Based on the fourth and fifth rows in (4), we can obtain

$$Ac_{34} + Bs_{34} = C \tag{5}$$

where $A = H - L_2c_2c_3$, $B = (L_1 - V - L_2s_3)c_2$, and $C = (L_3 + L_4)c_2 + \delta_2c_{34} + \delta_3c_2s_{34}$.

By defining $t = \tan\frac{q_3 + q_4}{2}$, we have

$$(A + C)t^2 - 2Bt + C - A = 0 \tag{6}$$

Then, we have

$$\tilde{q}_2 = q_3 + q_4 = 2\arctan\frac{B - \sqrt{A^2 + B^2 - C^2}}{A + C} \tag{7}$$

By using active exoskeleton joints q_2 and q_3 to constitute $\mathbf{q}_a = [q_2, q_3]^{\mathrm{T}}$, we have

$$\tilde{\mathbf{q}} = \mathbf{X}(\mathbf{q}_a, \boldsymbol{\delta}) \tag{8}$$

Equations (7) and (8) show that the human knee's forward kinematics may be affected by the relative displacements. With the assumption that the relative displacements are fixed for each user, the forward kinematics can be completely determined through the experimental identification of the relative displacements.

2) Inverse Kinematics of Knee Exoskeleton: The third and fourth rows in (4) yields

$$q_1 = \delta_1 + (H - \delta_2)t_{\tilde{q}_1} \tag{9}$$

where $t_{\tilde{q}_1} = \tan\tilde{q}_1$.

The third and fifth rows in (4) yields

$$q_3 = \arctan\frac{s_{\tilde{q}_1}(L_1 - V + (q_5 - L_5)c_{\tilde{q}_2} - (L_3 + L_4)s_{\tilde{q}_2} - \delta_3)}{q_1 - s_{\tilde{q}_1}((q_5 - L_5)s_{\tilde{q}_2} + (L_3 + L_4)c_{\tilde{q}_2}) - \delta_1} \tag{10}$$

where $s_{\tilde{q}_2} = \sin\tilde{q}_2$, $s_{\tilde{q}_1} = \sin\tilde{q}_1$, and $c_{\tilde{q}_2} = \cos\tilde{q}_2$.

Based on (9) and (10), q_3 can be expressed as a function of $\tilde{q}_1$ and $\tilde{q}_2$. Given that $q_2 = \tilde{q}_1$, $\mathbf{q}_a$ can be expressed as a function of $\tilde{q}_1$ and $\tilde{q}_2$. Thus, the inverse kinematics of the knee exoskeleton can be obtained.

B. Statics of Knee Exoskeleton

Considering the biological structural properties of the human knee, we assume that the displacements $(\delta_1, \delta_2, \delta_3)$ only change slowly; that is, $\dot{\boldsymbol{\delta}}_a = 0$. Based on the forward kinematics (8), we can obtain

$$\dot{\tilde{\mathbf{q}}} = \mathbf{J}(\mathbf{q}_a)\dot{\mathbf{q}}_a \tag{11}$$

where $\dot{\tilde{\mathbf{q}}}$ and $\dot{\mathbf{q}}_a$ represent the speed vectors of the human hip and knee joints and the active exoskeleton joints, respectively. $\mathbf{J}(\mathbf{q}_a)$ represents the Jacobian matrix, and it can be calculated according to forward kinematics (8). Then, we can obtain the following static equation using the virtual work method

$$\boldsymbol{\tau}_{\mathbf{q}_a} = \mathbf{J}^{\mathrm{T}}(\mathbf{q}_a)\boldsymbol{\tau}_{\tilde{\mathbf{q}}} \tag{12}$$

where $\boldsymbol{\tau}_{\mathbf{q}_a}$ and $\boldsymbol{\tau}_{\tilde{\mathbf{q}}}$ represent the torque vectors of the active exoskeleton joints and the human hip and knee joints, respectively. $\mathbf{J}$ is an abbreviation of $\mathbf{J}(\mathbf{q}_a)$.

C. Kinematic Compatibility Analysis of Knee Exoskeleton

The relative displacements $(\delta_1, \delta_2, \delta_3)$ caused by the misalignment of the human-robot joint axes may lead to a hyperstatic force in the exoskeleton-human system, harmful tissue deformation, and undesired forces or moments on the human limb. Fig. 3(b) depicts the force condition of the exoskeleton-human system. F_1 and F_2 are the two interaction forces exerted by the exoskeleton on the shank. These forces, when directed appropriately, can support the movement of the shank. F_3 is the constraint force along the shank, which may cause shear forces on the shank. τ_{a1}, τ_{a2}, and τ_{a3} are the constraint moments generated when the exoskeleton assists the movement of the shank. Among the above forces and moments, F_3, τ_{a1}, τ_{a2}, and τ_{a3} are undesired, they cannot be converted into useful work by the exoskeleton, and may cause damage to the human shank. To guarantee the safety of users, F_3, τ_{a1}, τ_{a2}, and τ_{a3} should be minimized or eliminated.

Based on the above analyses, the undesired forces or moments of the human limb are mainly caused by relative displacements $(\delta_1, \delta_2, \delta_3)$. According to the third to fifth items in (4), the relative displacements can be determined by the exoskeleton joints q_i ($i=1,\ldots,5$), where q_1, q_4, and q_5 are the passive joints of the exoskeleton. Thus, passive joints q_1, q_4, and q_5 can adapt to the relative displacements $(\delta_1, \delta_2, \delta_3)$, while guaranteeing the normal assisting function of the exoskeleton. τ_{a1}, τ_{a2} and τ_{a3} can be partially eliminated through the selection of a proper Velcro strap that allows for a slight rotation around the shank axis. The undesired force F_3 can be reduced by sliding joint q_5. In summary, the undesired forces and moments F_3, τ_{a1}, τ_{a2}, and τ_{a3} can be eliminated or reduced by the passive joints of the knee exoskeleton. Thus, the proposed knee exoskeleton possesses the capability for kinematic compatibility, allowing it to self-align with the human joint axes.

IV. MANIPULABILITY ANALYSIS AND OPTIMIZATION

A. Dynamic Modeling of the Knee Exoskeleton

In this paper, the Lagrange method [31] is used to establish the dynamic equation of the closed-loop system formed by the exoskeleton and the shank. The generalized coordinates are defined as $\Theta = \mathbf{q}_a$. Then, the dynamic model of the exoskeleton can be established as

$$\frac{d}{dt}\left(\frac{\partial L}{\partial \dot{\Theta}}\right) - \frac{\partial L}{\partial \Theta} = \mathbf{Q} \tag{13}$$

where $L = E - U$ represents the Lagrangian function; E and U represent the kinetic energy and potential energy, respectively; and $\mathbf{Q}$ represents the generalized force.

With the assumption the connecting links L_i ($i = 1, \ldots, 4$) of the exoskeleton and the shank are mass-concentrated, the closed-loop system's kinetic energy can be obtained as

$$E = \sum_{i=1}^{4}\left(\frac{1}{2}m_i v_{ci}^2\right) + \frac{1}{2}m_{\tilde{0}} v_{c_{\tilde{0}}}^2 \tag{14}$$

where m_i and $m_{\tilde{0}}$ are the concentrated mass of the exoskeleton and the human shank, respectively; v_{ci} and $v_{c_{\tilde{0}}}^2$ are the corresponding center-of-mass velocities. Since $\dot{q}_1$ and $\dot{q}_4$ are

determined by $\dot{q}_2$ and $\dot{q}_3$, the center-of-mass velocities can be obtained based on the modified D-H method.

The potential energy U of the closed-loop system is determined by gravity, which can be written as

$$U = \sum_{i=1}^{4} m_i g h_{ci} + m_{\tilde{0}} g h_{c_{\tilde{0}}} \tag{15}$$

where h_{ci} and $h_{c_{\tilde{0}}}$ are the center-of-mass position vectors of the exoskeleton and shank, respectively.

According to the Lagrangian method, the dynamic model of the exoskeleton can be established as

$$\mathbf{M}\ddot{\mathbf{q}}_a + \mathbf{C}\dot{\mathbf{q}}_a + \mathbf{G} + \mathbf{J}^{\mathrm{T}}\boldsymbol{\tau}_e = \boldsymbol{\tau}_{\mathbf{q}_a} \tag{16}$$

where $\mathbf{M}$ represents the inertia matrix, and $\mathbf{C}$ represents the damping matrix. According to (16), the dynamics of the exoskeleton can be determined by the torque vector $\boldsymbol{\tau}_{\mathbf{q}_a}$ of the active exoskeleton joints.

B. Torque Manipulability Index of Knee Exoskeleton

By taking the derivative of (11), we can get

$$\ddot{\tilde{\mathbf{q}}} = \mathbf{J}\ddot{\mathbf{q}}_a + \dot{\mathbf{J}}\dot{\mathbf{q}}_a \tag{17}$$

The motion torque relationship of the shank is

$$\boldsymbol{\tau}_e = \mathbf{M}_e \ddot{\tilde{\mathbf{q}}} + \boldsymbol{\tau}_g \tag{18}$$

where $\boldsymbol{\tau}_e = [\tau_{\tilde{q}_1}, \tau_{\tilde{q}_2}]^{\mathrm{T}}$, $\mathbf{M}_e$ is the pseudo-inertia matrix of the shank, and $\boldsymbol{\tau}_g$ is the torque vector induced by gravity.

Then, (16) can be transformed into

$$\mathbf{B}\boldsymbol{\tau}_e + \boldsymbol{\delta} = \boldsymbol{\tau}_{\mathbf{q}_a} \tag{19}$$

where $\mathbf{B} = \mathbf{M}\mathbf{J}^{-1}\mathbf{M}_e^{-1} + \mathbf{J}^{\mathrm{T}}(\mathbf{q}_a)$, and $\boldsymbol{\delta} = -\mathbf{M}\mathbf{J}^{-1}\mathbf{M}_e^{-1}\boldsymbol{\tau}_g - \mathbf{M}\mathbf{J}^{-1}\dot{\mathbf{J}}\dot{\mathbf{q}}_a + \mathbf{C}\dot{\mathbf{q}}_a + \mathbf{G}$.

The torque limit of the exoskeleton joints is $\left|\tau_{q_{ai}}\right| \leq \tau_{q_{ai},\max}$ ($i = 1, 2$), where $\tau_{q_{a1}} = \tau_{q_2}$ and $\tau_{q_{a2}} = \tau_{q_3}$, and $\tau_{q_{ai},\max}$ is the maximum of the i-th active joint torque. The weight matrix is defined as $\mathbf{W}_\tau = \mathrm{diag}[1/\tau_{q_{a2},\max}, 1/\tau_{q_{a3},\max}]$. The scaled joint moments are defined as $\tilde{\boldsymbol{\tau}}_{\mathbf{q}_a} = \mathbf{W}_\tau \boldsymbol{\tau}_{\mathbf{q}_a}$. The manipulability of the scaled joint torque is defined as $\tilde{\boldsymbol{\tau}}_{\mathbf{q}_a}^{\mathrm{T}} \tilde{\boldsymbol{\tau}}_{\mathbf{q}_a} \leq 1$. The torque variation range of the exoskeleton is

$$(\mathbf{B}\boldsymbol{\tau}_e + \boldsymbol{\delta})^{\mathrm{T}} \mathbf{W}_\tau^{\mathrm{T}} \mathbf{W}_\tau (\mathbf{B}\boldsymbol{\tau}_e + \boldsymbol{\delta}) \leq 1 \tag{20}$$

To represent the torque transfer capability from exoskeleton joint moments to human knee joint moments, the local torque manipulability metric can be expressed as

$$w_\tau = \sqrt{\det\left(\mathbf{B}^{\mathrm{T}}\mathbf{W}_\tau^{\mathrm{T}}\mathbf{W}_\tau \mathbf{B}\right)^{-1}} \tag{21}$$

Based on (21), a global torque manipulability (GTM) index $w_{g\tau}$ is proposed to evaluate the torque transmission ability of the exoskeleton. The index can be expressed as

$$w_{g\tau} = \frac{\int_W w_\tau \, dW}{\int_W dW} \tag{22}$$

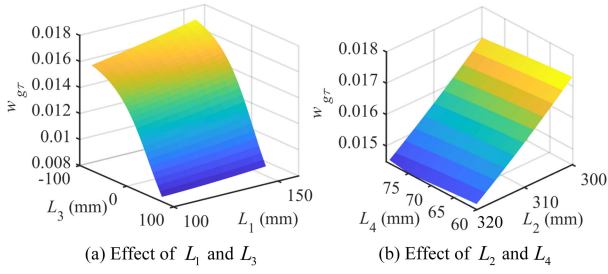where $\int_W dW = \iint d\tilde{q}_1 d\tilde{q}_2$.

(a) Effect of L_1 and L_3 (b) Effect of L_2 and L_4

Fig. 4.   Effects of dimensional parameters L_i (i=1,...,4) on GTM.

(a) Without the exoskeleton   (b) With the exoskeleton

Fig. 5.   Experimental setup to test the limb movements. (a) Without the exoskeleton. (b) With the exoskeleton.

C. Manipulability Analysis of Knee Exoskeleton

Based on the physical prototype, we set the dimensional parameters of the knee exoskeleton in the analyses. The basic dimensional parameters of the knee exoskeleton are set to $L_1 = 140$ mm, $L_2 = 300$ mm, $L_3 = -73$ mm, $L_4 = 75$ mm, $L_5 = 200$ mm, $V = 200$ mm, and $H = 200$ mm. The masses of the exoskeleton are set to $m_1 = 300$ g, $m_2 = 200$ g, $m_3 = 400$ g, and $m_4 = 500$ g. The inertia matrix of the exoskeleton can be calculated by

$$\mathbf{M}_e = \begin{bmatrix} \frac{1}{12}m_e\left(3R^2 + h^2\right) & 0 \\ 0 & \frac{1}{12}m_e\left(3R^2 + h^2\right) \end{bmatrix} \quad (23)$$

where R and h are the diameter and length of the shank, and m_e is the estimated mass of the shank with $R = 50$ mm, $h = 200$ mm, and $m_e = 1000$ g.

The motion ranges of joints $\tilde{q}_1$ and $\tilde{q}_2$ are set to $-20° \leq \tilde{q}_1 \leq 20°$ and $0° \leq \tilde{q}_2 \leq 90°$. With $L_2 = 300$ mm, $L_4 = 60$ mm, 100 mm $\leq L_1 \leq 150$ mm, and -75 mm $\leq L_3 \leq 75$ mm, Fig. 4(a) shows the effects of parameters L_1 and L_3 on $w_{g\tau}$. With $L_1 = 140$ mm, $L_3 = -75$ mm, 300 mm $\leq L_2 \leq 320$ mm, and 60 mm $\leq L_4 \leq 80$ mm, Fig. 4(b) shows the effects of parameters L_2 and L_4 on $w_{g\tau}$. According to Fig. 4, the dimensional parameters of the knee exoskeleton affect the GTM index $w_{g\tau}$ by a factor greater than 1, thereby influencing the torque transmission capability of the exoskeleton.

D. Optimization of the Knee Exoskeleton

To obtain the optimal dimensional parameters of the exoskeleton, $L_1 = 140$ mm is selected based on experience. The variable to be optimized is selected as $x = [L_2, L_3, L_4]^T$, so that the objective optimization problem becomes

$$\min 1/w_{g\tau} \quad (24)$$

subjected to

$$\begin{cases} 300\text{mm} \leq L_2 \leq 320\text{mm} \\ -75\text{mm} \leq L_3 \leq -35\text{mm} \\ 60\text{mm} \leq L_4 \leq 80\text{mm} \end{cases} \quad (25)$$

The genetic algorithm 'ga' in MATLAB is used to solve the optimization problem, and the parameters are set as follows: $PopulationSize = 30$, $Generations = 100$, $StallGenLimit = 100$, $MigrationFraction = 0.05$, and $CrossoverFraction = 0.95$. Then, the optimal GTM index $w_{g\tau}$ and optimal results can be obtained. The optimal dimensional parameters of the exoskeleton are L_2=300 mm, $L_3 = -35$ mm, and L_4=80 mm, and the optimal GTM index $w_{g\tau}$ converges to 0.06.
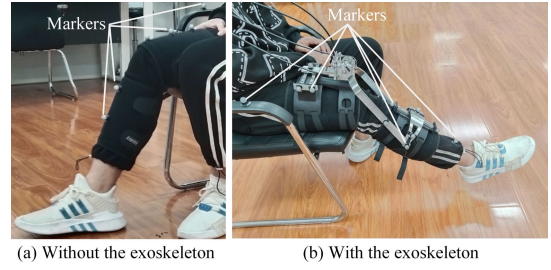
V. EXPERIMENTAL VALIDATION

Comprehensive experiments were conducted to verify the performance of the proposed exoskeleton. First, the exoskeleton's kinematic transparency was tested using a motion capture system. Second, an experiment was conducted to show the range of motion (ROM) of the exoskeleton. Third, an interaction force experiment was conducted to test the interaction performance of the exoskeleton. Fourth, a motion-assistance experiment was performed to verify the task-assistance capability of the exoskeleton.

A. Kinematic Transparency Experiment

A motion capture system (Vicon, USA) equipped with twelve cameras was used to measure the motion trajectories of the knee exoskeleton. The maximum sampling frequency can reach 180 Hz, and the average measurement accuracy is 0.1 mm. As shown in Fig. 5, several markers were placed on the thigh and shank to measure the angles of the knee FE and hip IER. Five healthy participants (three men, and two women) were selected for this experiment. The age, height, and weight of these participants were 22-35 years old, 155-185 cm, and 55-95 kg, respectively. To test the kinematic performance of the exoskeleton, two actions were performed by the participants or the exoskeleton. First, the participants were instructed to perform knee FE and hip IER movements. The ranges of motion for the knee FE and hip IER movements were 100º and 20º, respectively. The motion period was 12 s, and the motion speed was controlled to make the motion as smooth as possible. Second, based on the experimental data of the above movements, we designed the motion trajectories of the exoskeleton and used the angle position control to assist the participants in performing the knee FE and hip IER movements [25]. Each movement has been repeated five times in this experiment.

Based on the experimental data, by using the geometrical algorithm [25], the trajectories of the five participants' hip IER and knee FE movements are depicted in Fig. 6. The hip IER and knee FE movements in the case with the knee exoskeleton were similar to those in the case without the knee exoskeleton. In addition, the Pearson's correlation coefficients (PCC) of the knee FE and hip IER movements for the five participants were obtained according to the experimental data. The average PCC of the knee FE and hip IER movements were 0.9231 and 0.8977, respectively. That is, a strong correlation' existed between the motions with and without the exoskeleton. Thus, when the participants wore the exoskeleton, the knee exoskeleton could assist the participant in performing the motion
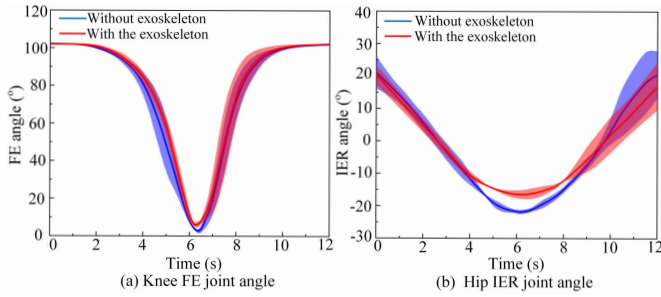
Fig. 6. Trajectories of the knee FE and hip IER joint angles with and without the exoskeleton.
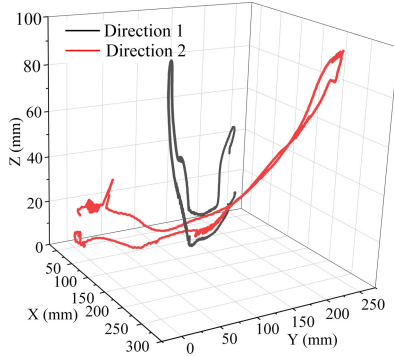

Fig. 7. Trajectories generated by the simultaneous rotations of the knee FE and hip IER motion in different directions.
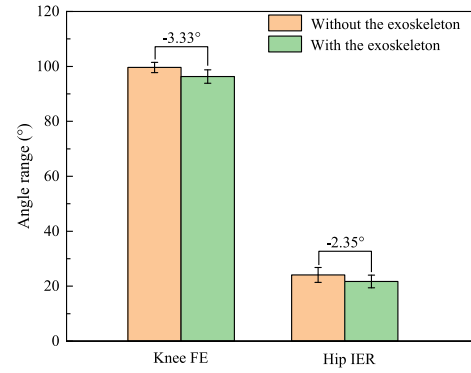

Fig. 8. ROM results of the knee exoskeleton.

exoskeleton joint q_2 was set to stationary. Thus, the exoskeleton can be used to assist the knee FE movement through angle control, and the motion curves of passive joints q_1, q_4, and q_5 can be recorded. Fig. 9 displays the motion curves of passive rotary joint q_4 and passive sliding joints q_1 and q_5. The experimental results shows that the exoskeleton generated self-aligning motions of passive joints when assisting the participants in performing the corresponding movements. That is, the exoskeleton can adapt to the variations in the knee's instantaneous rotation center. In addition, as shown in Eq. (7), human-robot misalignment can induce motion in passive joints. Both the theoretical and experimental results of the exoskeleton demonstrate the capability of the knee exoskeleton to align with the rotational axes of the human body.

D. Interaction Force Experiment

The interaction force/torque signals were recorded through a six-axis force/torque sensor (ATI Gamma, USA) installed on the shank. The directions of the forces and torques of the force/torque sensor have been shown in Fig. 1(a). When the sliding joint q_1 at the thigh was unlocked and the exoskeleton joint q_2 was fixed by the motor, the exoskeleton functioned as a planar self-aligning knee exoskeleton with an RRP mechanism. This mechanism configuration resembled the Utah Exoknee exoskeleton, which also features an RRP mechanism [24]. In addition, as shown in Fig. 10, a traditional unicentric knee exoskeleton was fabricated, whose joint was actuated by the Bowden cable. Its cable transmission system was identical to that of the proposed exoskeleton.

First, the knee FE assistance experiment was performed on the same five participants as those in the kinematic transparency experiment. The desired trajectories of the exoskeleton joints q_2 and q_3 were set to $q_2 = 0$ and $q_3 = 100° \cos(0.26t)$. The experiments were repeated five times. The experimental results illustrating the interaction forces and torques during the assisted knee FE movement are depicted in Fig. 11. The absolute value of the mean value of each force or torque is denoted as AM. The arithmetic square root of the sum of the squares of the AM for three forces or torques is denoted as the force or torque SRAM. The results of the AMs of the three exoskeletons are given in Fig. 12. The AMs of F_x, F_y, F_z, T_x, T_y, and T_z of the developed exoskeleton were 38.8%, 2.0%, 8.0%, 53.7%, 11.5%, and 10.6% lower than those of the planar self-aligning exoskeleton. Additionally, the AMs for the developed exoskeleton were 89.8%, 73.1%, 14.1%,
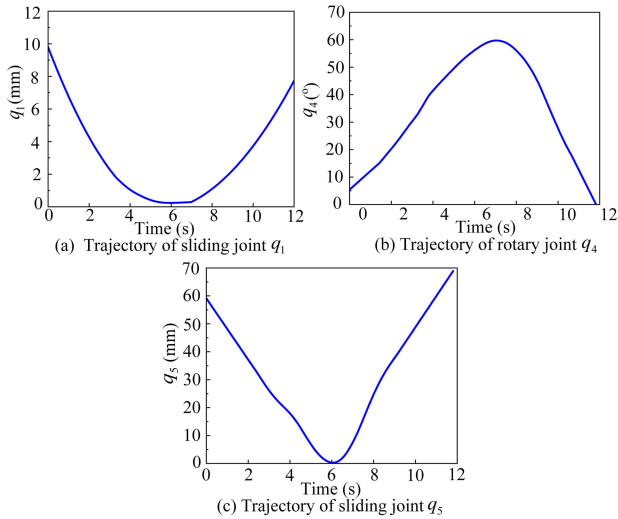
trajectory that approximates the natural motion trajectory of the participant without the exoskeleton. This experimental result shows the knee exoskeleton had good performance in terms of kinematic transparency. Fig. 7 depicts the trajectories of a marker on the participant's shank near the ankle when the knee exoskeleton was used to assist the simultaneous movement of hip IER and knee FE. The trajectories in Fig. 7 show that the knee exoskeleton can simultaneously assist in knee FE and hip IER movements.

B. Range of Motion

The ROMs of human joints with the exoskeleton can be influenced by the attachment of the device's wearing strap and the dimensions of the limbs. According to the experimental data in Fig. 6, the ROMs of the hip IER and knee FE movements in the cases with and without the knee exoskeleton were calculated, and the ROMs were analyzed. Fig. 8 presents the ROM results for the five participants. The ROMs of the knee FE in the cases without and with the knee exoskeleton were $99.62° \pm 0.78°$ and $96.29° \pm 0.81°$, respectively. The difference in the above two ROMs of the knee FE was statistically significant ($p = 0.0032$). The ROMs of the hip IER without and with the knee exoskeleton were $24.08° \pm 0.91°$ and $21.73° \pm 0.77°$, respectively. The difference in the above two ROMs of the hip IER was statistically significant ($p = 0.0041$). The experimental result shows that the reduction in ROM when the participant wore the exoskeleton was slight. Thus, the proposed knee exoskeleton can engage in natural motions of the human hip IER and knee FE.

C. Self-Aligning Experiment

In the self-aligning experiment, the desired trajectory of the exoskeleton joint q_3 was set to $q_3 = 100° \cos(0.26t)$; and the

Fig. 9. Trajectories of sliding joint q_1, rotary joint q_4, and sliding joint q_5.

Fig. 10. Traditional unicentric knee exoskeleton.

87.0%, 79.1%, and 16.3% lower than those of the unicentric exoskeleton. Furthermore, the force and torque SRAMs for the developed exoskeleton were calculated to be 8.1% and 26.4% lower than those of the planar self-aligning exoskeleton and were 28.1% and 72.1% lower than those of the traditional unicentric exoskeleton. The difference in SRAMs between the developed exoskeleton and the planar self-aligning exoskeleton was statistically significant ($p = 0.0024$). Similarly, the variance in SRAMs between the developed and unicentric exoskeletons was statistically significant ($p = 0.0019$).

Second, the hip IER assistance experiment was performed in cases with the shank slider unlocked and locked on the above five participants. The desired trajectories of the exoskeleton joints q_2 and q_3 were set to $q_2 = 20° \cos(0.26t)$ and $q_3 = 0$. The experiments were repeated five times. The experimental results for the hip IER movement assistance are depicted in Fig. 13, and the AM results in both unlocked and locked states are presented in Fig. 14. The AMs of F_x, F_y, F_z, T_x, T_y, and T_z in the unlocked state were 30.5%, 8.0%, 33.7%, 47.8%, 28.6%, and 44.8% lower than those in the locked state. The force and torque SRAMs of the developed exoskeleton in the unlocked state were calculated to be 6.4% and 45.7% lower than those in the locked state. The difference in SRAMs between the interaction forces and torques of the developed exoskeleton in the unlocked state and those of the exoskeleton in the locked state was also statistically significant ($p = 0.0022$).

Based on the force/torque sensor and the motion capture system, Fig. 15 presents a curve of the torque generated by the exoskeleton to assist participants during knee FE experiments.
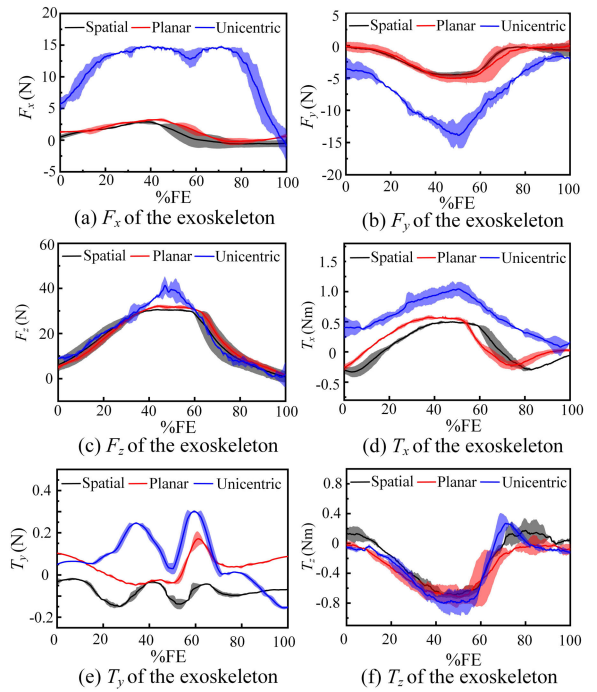

Fig. 11. Experimental results of the interaction forces and torques for the knee FE assistance. %FE represents the percentage of the task progress.
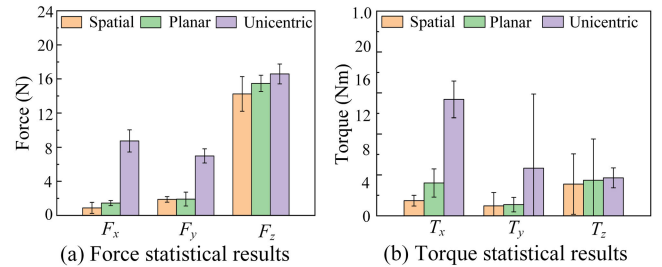

Fig. 12. Statistical results of the AM values of the interaction forces and torques during the knee FE movement assistance.

The torque experimental data shows that the exoskeleton can provide a large assistance torque of up to 86.5 Nm.

E. Motion Assistance Experiment

To demonstrate the performance of the knee exoskeleton in terms of motion assistance, we used the knee exoskeleton to actively assist the participant in completing the knee FE movement and hip IER movement. The motion processes of the participant during the experiments are shown in Fig. 16. Figure 16(a) illustrates the motion processes involved in assisting the participant to perform the knee FE movement. Fig. 16(b) shows the motion processes involved in assisting the participant to complete the hip IER movement. The experimental results demonstrated that the proposed knee exoskeleton can perform the knee FE and hip IER assistance.

VI. DISCUSSION AND FUTURE WORK

The advantages of the proposed knee exoskeleton are summarized here. Different from the planar knee exoskeletons [17], [18], [19], [20], [21], [22], [23], this paper proposes a novel spatial self-aligning mechanism that endows the knee exoskeleton with the capability to simultaneously assist in
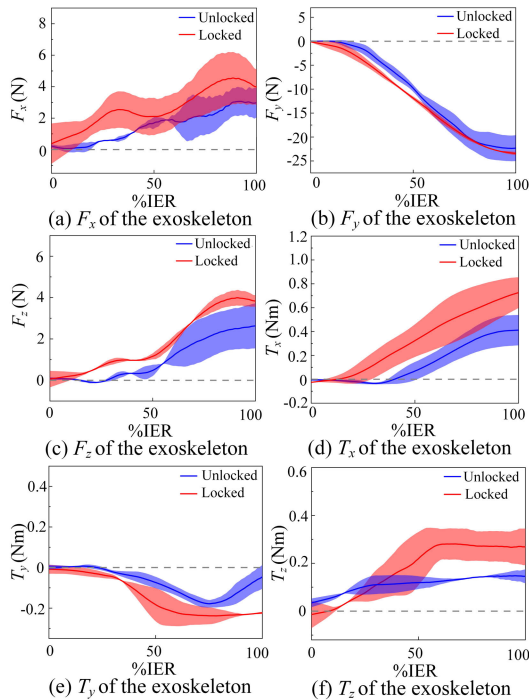
Fig. 13. Experimental results of the interaction forces and torques for the hip IER assistance. %IER represents the percentage of the task progress.
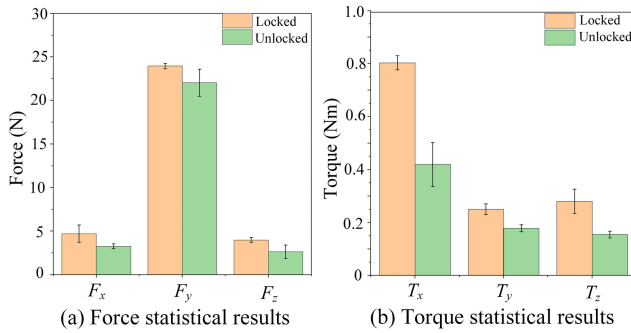

Fig. 14. Statistical analysis results of the AM values of the interaction forces and torques during the hip IER assistance.

knee FE and hip IER movements. To the authors' knowledge, this study marks the first design of an exoskeleton that simultaneously supports knee FE and hip IER movements. The primary advantage of the exoskeleton is its independent motion-assistance capability. Given the exoskeleton's ability to independently assist in each degree of freedom of the participants' joints, it holds the potential for enhancing rehabilitation effects [29]. Additionally, the experiments shows that the force and torque SRAMs of the developed exoskeleton were 8.1% and 26.4% lower than those of the planar self-aligning exoskeleton [22], [23] and were 28.1% and 72.1% lower than those of the unicentric exoskeleton. Reducing interaction forces has been shown to improve participants' comfort [23]. According to the above result, the proposed exoskeleton can offer better wearing comfort than traditional designs. In future research, we will further evaluate the comfort of participants wearing the proposed exoskeleton, to demonstrate the extent of improvement in comfort levels.
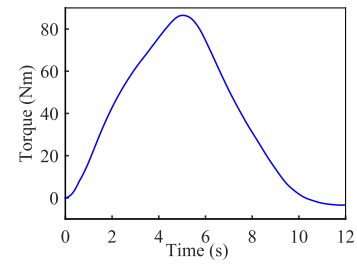

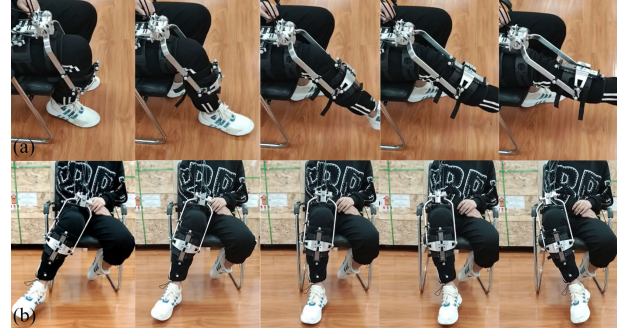Fig. 15. Torque curve that the exoskeleton provided to the participant.

Fig. 16. Motion assistance experiment of the knee exoskeleton. (a) Assist the participant to complete the knee FE movement. (b) Assist the participant to complete the hip IER movement.

Despite the benefits of the proposed knee exoskeleton, it is still characterized by some limitations. First, the human-robot interface of the knee exoskeleton is relatively simplistic and does not fully incorporate ergonomic principles. There is room for improvement in the design of the human-computer interface. Second, relative displacements may arise due to variations in human lower limb sizes and soft tissue deformations. While relative displacements caused by human lower limb sizes are constant for each participant, those induced by soft tissue deformations fluctuate over time within a small range. Hence, the complete determination of the forward kinematics of the knee exoskeleton may require corresponding assumptions, potentially resulting in additional degrees of freedom (DOFs). Because the variable component of the relative displacement is typically quite small, the additional DOFs will have limited effects on the exoskeleton control, as confirmed by assistance experiments. In future research, adaptive control methods will be further developed to accommodate variable relative displacements for more accurate control of the human limb. Third, owing to the difficulty in obtaining the actual relative displacements of the human knee joint, it is difficult to quantitatively compare passive joints' trajectories obtained using the theoretical model with those obtained via experiments. Further study is needed to develop quantitative methods for evaluating the self-aligning ability of the exoskeleton. Fourth, the comparison of the proposed knee exoskeleton with the traditional knee exoskeleton in terms of their ability to reduce the required motor forces remains unclear and should be further studied in future work.

VII. CONCLUSION

This paper proposed a novel spatial self-aligning mechanism for a knee exoskeleton to enable simultaneous assistance

in knee FE and hip IER motions. The kinematic compatibility of the knee exoskeleton was analyzed, and the knee exoskeleton was optimized based on a GTM index. Experiments were conducted to verify the performance of the proposed exoskeleton concerning knee FE and hip IER movements. First, the exoskeleton's kinematic transparency was verified through the calculation of the average PCC of the knee FE and hip IER movements. Second, the ROM of the knee exoskeleton was tested to demonstrate its capacity to assist in most of the natural motions of knee FE and hip IER. Third, an interaction force experiment was conducted to test the interaction performance of the exoskeleton. The experimental results of the knee FE assistance show that the force and torque SRAMs of the developed exoskeleton were 8.1% and 26.4% lower than those of the planar self-aligning exoskeleton and were 28.1% and 72.1% lower than those of the traditional unicentric exoskeleton. The experimental results of the hip IER assistance show that the force and torque SRAMs of the developed exoskeleton in the unlocked state were 6.4% and 45.7% lower than those in the locked state. Fourth, a motion-assistance experiment was performed to verify the task-assistance capability of the exoskeleton. In conclusion, the comprehensive performance of the proposed knee exoskeleton was validated in terms of the kinematic transparency, ROM, interaction forces and torques, and motion assistance.

REFERENCES

[1] K.-M. Lee and J. Guo, "Kinematic and dynamic analysis of an anatomically based knee joint," *J. Biomech.*, vol. 43, no. 7, pp. 1231–1236, May 2010.

[2] J. Wismans, F. Veldpaus, J. Janssen, A. Huson, and P. Struben, "A three-dimensional mathematical model of the knee-joint," *J. Biomech.*, vol. 13, no. 8, pp. 677–685, Jan. 1980.

[3] M. De Carlo and B. Armstrong, "Rehabilitation of the knee following sports injury," *Clinics Sports Med.*, vol. 29, no. 1, pp. 81–106, Jan. 2010.

[4] T. Alif, S. Bhasin, K. Garg, and D. Joshi, "An enhanced model free adaptive control approach for functional electrical stimulation assisted knee joint regulation and control," *IEEE Trans. Neural Syst. Rehabil. Eng.*, vol. 31, pp. 1584–1593, 2023.

[5] Z. Wang et al., "Knee flexion-assisted method for human-exoskeleton system," *IEEE Trans. Neural Syst. Rehabil. Eng.*, vol. 31, pp. 2800–2808, 2023, doi: 10.1109/TNSRE.2023.3287867.

[6] W. S. Barrutia, J. Bratt, and D. P. Ferris, "A human lower limb mechanical phantom for the testing of knee exoskeletons," *IEEE Trans. Neural Syst. Rehabil. Eng.*, vol. 31, pp. 2497–2506, 2023.

[7] B. Chen, B. Zi, Z. Wang, L. Qin, and W.-H. Liao, "Knee exoskeletons for gait rehabilitation and human performance augmentation: A state-of-the-art," *Mechanism Mach. Theory*, vol. 134, pp. 499–511, Apr. 2019.

[8] R. R. Torrealba, S. B. Udelman, and E. D. Fonseca-Rojas, "Design of variable impedance actuator for knee joint of a portable human gait rehabilitation exoskeleton," *Mechanism Mach. Theory*, vol. 116, pp. 248–261, Oct. 2017.

[9] D. Lee, B. McLain, I. Kang, and A. Young, "Biomechanical comparison of assistance strategies using a bilateral robotic knee exoskeleton," *IEEE Trans. Biomed. Eng.*, vol. 68, no. 9, pp. 2870–2879, Sep. 2021.

[10] K. Shamaei, M. Cenciarini, A. A. Adams, K. N. Gregorczyk, J. M. Schiffman, and A. M. Dollar, "Design and evaluation of a quasi-passive knee exoskeleton for investigation of motor adaptation in lower extremity joints," *IEEE Trans. Biomed. Eng.*, vol. 61, no. 6, pp. 1809–1821, Jun. 2014.

[11] T.-H. Huang et al., "Modeling and stiffness-based continuous torque control of lightweight quasi-direct-drive knee exoskeletons for versatile walking assistance," *IEEE Trans. Robot.*, vol. 38, no. 3, pp. 1442–1459, Jun. 2022.

[12] B. Zhong et al., "A cable-driven exoskeleton with personalized assistance improves the gait metrics of people in subacute stroke," *IEEE Trans. Neural Syst. Rehabil. Eng.*, vol. 31, pp. 2560–2569, 2023.

[13] D. Zanotto, Y. Akiyama, P. Stegall, and S. K. Agrawal, "Knee joint misalignment in exoskeletons for the lower extremities: Effects on user's gait," *IEEE Trans. Robot.*, vol. 31, no. 4, pp. 978–987, Aug. 2015.

[14] E. J. Park et al., "A hinge-free, non-restrictive, lightweight tethered exosuit for knee extension assistance during walking," *IEEE Trans. Med. Robot. Bionics*, vol. 2, no. 2, pp. 165–175, May 2020.

[15] Z. Wang, Z. Zhou, L. Ruan, X. Duan, and Q. Wang, "Mechatronic design and control of a rigid-soft hybrid knee exoskeleton for gait intervention," *IEEE/ASME Trans. Mechatronics*, vol. 28, no. 5, pp. 2553–2564, Oct. 2023.

[16] A. H. A. Stienen, E. E. G. Hekman, F. C. T. van der Helm, and H. van der Kooij, "Self-aligning exoskeleton axes through decoupling of joint rotations and translations," *IEEE Trans. Robot.*, vol. 25, no. 3, pp. 628–633, Jun. 2009.

[17] D. Wang, K.-M. Lee, J. Guo, and C.-J. Yang, "Adaptive knee joint exoskeleton based on biological geometries," *IEEE/ASME Trans. Mechatronics*, vol. 19, no. 4, pp. 1268–1278, Aug. 2014.

[18] M. A. Ergin and V. Patoglu, "A self-adjusting knee exoskeleton for robot-assisted treatment of knee injuries," in *Proc. IEEE/RSJ Int. Conf. Intell. Robots Syst.*, Sep. 2011, pp. 4917–4922.

[19] L. Saccares, I. Sarakoglou, and N. G. Tsagarakis, "IT-knee: An exoskeleton with ideal torque transmission interface for ergonomic power augmentation," in *Proc. IEEE/RSJ Int. Conf. Intell. Robots Syst. (IROS)*, Oct. 2016, pp. 780–786.

[20] Y. Lee et al., "Biomechanical design of a novel flexible exoskeleton for lower extremities," *IEEE/ASME Trans. Mechatronics*, vol. 22, no. 5, pp. 2058–2069, Oct. 2017.

[21] J. Wang et al., "Comfort-centered design of a lightweight and back-drivable knee exoskeleton," *IEEE Robot. Autom. Lett.*, vol. 3, no. 4, pp. 4265–4272, Oct. 2018.

[22] S. V. Sarkisian, M. K. Ishmael, G. R. Hunt, and T. Lenzi, "Design, development, and validation of a self-aligning mechanism for high-torque powered knee exoskeletons," *IEEE Trans. Med. Robot. Bionics*, vol. 2, no. 2, pp. 248–259, May 2020.

[23] S. V. Sarkisian, M. K. Ishmael, and T. Lenzi, "Self-aligning mechanism improves comfort and performance with a powered knee exoskeleton," *IEEE Trans. Neural Syst. Rehabil. Eng.*, vol. 29, pp. 629–640, 2021.

[24] M. Cempini, S. M. M. De Rossi, T. Lenzi, N. Vitiello, and M. C. Carrozza, "Self-alignment mechanisms for assistive wearable robots: A kinetostatic compatibility method," *IEEE Trans. Robot.*, vol. 29, no. 1, pp. 236–250, Feb. 2013.

[25] P. Agarwal, Y. Yun, J. Fox, K. Madden, and A. D. Deshpande, "Design, control, and testing of a thumb exoskeleton with series elastic actuation," *Int. J. Robot. Res.*, vol. 36, no. 3, pp. 355–375, Mar. 2017.

[26] N. Sun, G. Li, and L. Cheng, "Design and validation of a self-aligning index finger exoskeleton for post-stroke rehabilitation," *IEEE Trans. Neural Syst. Rehabil. Eng.*, vol. 29, pp. 1513–1523, 2021.

[27] G. Li, L. Cheng, Z. Gao, X. Xia, and J. Jiang, "Development of an untethered adaptive thumb exoskeleton for delicate rehabilitation assistance," *IEEE Trans. Robot.*, vol. 38, no. 6, pp. 3514–3529, Dec. 2022.

[28] P. W. Duncan et al., "Management of adult stroke rehabilitation care: A clinical practice guideline," *Stroke*, vol. 36, no. 9, pp. e100–e143, Sep. 2005.

[29] V. Monaco, G. Galardi, M. Coscia, D. Martelli, and S. Micera, "Design and evaluation of NEUROBike: A neurorehabilitative platform for bedridden post-stroke patients," *IEEE Trans. Neural Syst. Rehabil. Eng.*, vol. 20, no. 6, pp. 845–852, Nov. 2012.

[30] X. Wang, S. Guo, B. Qu, and S. Bai, "Design and experimental verification of a hip exoskeleton based on human–machine dynamics for walking assistance," *IEEE Trans. Hum.-Mach. Syst.*, vol. 53, no. 1, pp. 85–97, Feb. 2023.

[31] G. Li, L. Cheng, and N. Sun, "Design, manipulability analysis and optimization of an index finger exoskeleton for stroke rehabilitation," *Mechanism Mach. Theory*, vol. 167, Jan. 2022, Art. no. 104526.